Quantitation of multiple sclerosis lesion volumes on magnetic resonance imaging

Ponnada A. Narayana*, Barry J. Bedell and Jerry S. Wolinsky†

Department of Radiology, †Department of Neurology, University of Texas at Houston Medical School, 6431 Fannin, Houston, TX 77030, USA

Multiple sclerosis is the most common demyelinating disease. Currently a number of clinical trials are underway for treating this disease. MRI-defined lesion burden is considered to be an useful marker for evaluating the efficacy of treatment. Quantitation of lesion burden in a clinical trial involving a large number of images requires a technique with minimal manual intervention. In this brief review we describe segmentation techniques, that are used in our laboratory, for automatic quantitation of lesion burden. A brief review of the novel pulse sequences for generating images with superior lesion-to-tissue contrast required for automatic lesion quantitation is also presented.

NEURAL tissue volumetry can provide fundamental information about the development and function of normal human brain and can yield important clues regarding the underlying pathology in patients[1,2]. For instance, valuable information has been gained about the pathological processes in epilepsy[3] and Alzheimer's disease[4] from the volume measurements of various structures in the brain. In many focal diseases such as multiple sclerosis (MS) and some cancers, the total lesion volume is thought to reflect the overall disease burden and therefore may be useful for quantitating the disease and objectively evaluating the effect of therapeutic intervention[5,6].

Quantitative tissue volumetry is commonly based on radiologic images. Different tissues are identified on the images, either manually or assisted by computer, for computing the volumes. The process of identifying and isolating a given tissue is generally referred to as segmentation. Segmentation allows for colour coding of different tissues for improved delineation and ease of visual identification of pathology. Segmentation is also useful in radiation therapy[7] and for simulating sensitive procedures for interventional neurosurgery[8,9].

Segmentation is the most critical step in quantitating tissue volumes. The ability to accurately segment and quantitate a given tissue volume critically depends on the contrast-to-noise ratio on the image. The introduction of magnetic resonance imaging (MRI) into the clinical arena has greatly increased the interest in tissue segmentation for at least two reasons. Firstly, MRI provides superb soft tissue contrast which allows clear identification and segmentation of different soft tissues. For instance, it is very easy to distinguish gray matter (GM), white matter (WM), and cerebrospinal fluid (CSF) in brain MRI. Secondly, MRI is a multi-parametric modality in the sense that tissue contrast can be altered by simply changing the scan parameters or pulse sequences. This multi-parametric nature of MRI plays a crucial role in image segmentation.

The focus of this review is on the quantitation of MS lesions in the brain and reflects our own research interest. MS is the most common demyelinating disease in humans[10]. It is a complex disease with a relapsing remitting course[11]. MRI is the radiologic modality of choice for non-invasively visualizing lesions and clinically following MS patients. Recent studies suggest that MRI is capable of detecting sub-clinical activity[12] and that MRI-defined lesion burden (or total lesion volume) may provide an objective measure of the disease severity. Therefore, there is a considerable interest in using MRI-estimated quantitative lesion load as an outcome measure in clinical trials[13–17]. Such an outcome measure can considerably reduce the cost of conducting clinical trials since fewer patients are required to achieve statistical significance. This is particularly relevant in view of a large number of ongoing clinical trials for treating MS patients.

Segmentation techniques

Segmentation involves the classification of tissues on images. Segmentation can be performed using a variety of techniques that have been recently reviewed[18–21]. Of all these techniques, three methods have been predominantly employed for segmentation of MS lesions[17]. These are (1) manual tracing, (2) intensity-based single image segmentation, and (3) multi-spectral methods. Both manual tracing and thresholding are simple to use and require relatively little additional software development. However, these techniques are prone to operator bias, time consuming, and impractical for analysing a large number of images[5,22–27]. The accuracy of these techniques depends on how rigorously the quality control is maintained.

*For correspondence. (e-mail: pan@msrad72.med.uth.tmc.edu)

Multispectral techniques

A unique feature of MRI is the ability to alter the relative contrast of tissues simply by manipulating the pulse sequences and/or pulse sequence parameters. For instance, both MS lesions and CSF appear bright on T_2-weighted spin echo images. On the other hand, MS lesions appear bright on density-weighted images while CSF appears somewhat isointense with the rest of the brain parenchyma. In T_1-weighted images lesions generally appear isointense with the parenchyma and CSF appear hypointense. Multispectral segmentation techniques, which are based on multiple image sets, exploit the powerful multi-parametric nature of MRI. In contrast, both manual tracing and thresholding are performed using a single set of images. The multi-spectral segmentation techniques are generally more robust since they combine information from multiple image sets with different contrast for tissue classification.

The concept of multi-spectral segmentation was originally developed for classification of the earth surface, based on images acquired with LANDSAT[28]. LANDSAT is the name used by NASA for satellites designed for monitoring the earth's resources. The sensors of LANDSAT acquire images at different spectral regions (wavelengths). Each frame of the LANDSAT imagery consists of four images of the same scene acquired in the red, green, and two infrared spectral regions. The segmented image is then generated by combining information from all four images. Similar multi-spectral techniques can be applied, by combining data from multiple MR images with different contrasts to classify an image into different tissue classes[29]. The input images used for tissue classification are referred to as 'features'. The pixel intensities of the basis set of images are generally referred to as 'feature vectors'. Multi-spectral segmentation can be performed either by 'feature space-based' or by 'non-feature space-based' methods. In this article, only the feature space-based techniques will be discussed. Artificial neural network-based techniques[30], adaptive segmentation[31] and model based techniques[32] which have been recently proposed will not be included in this review.

In the feature-based, multi-spectral segmentation technique, the feature vector is typically plotted in a n-dimensional space, referred to as the 'feature space', where n is the number of image sets. For instance, $n = 2$, if dual echo images are used for segmentation. In a two-dimensional (2D) feature space, the abscissa corresponds to the pixel intensities in one image, while the ordinate corresponds to intensities in the second image. In an ideal case, one can see clear clustering of different tissues in the feature space. Based on these clusters, it is possible to classify different tissues and calculate the individual volumes. Each tissue is assigned an arbitrary, but unique, colour for visual inspection of the images. In reality, due to limited tissue contrast and image noise, considerable overlap exists between these clusters, resulting in some ambiguity in the tissue classification.

Feature space classification

Due to the considerable overlap between different tissues in the feature space, it is essential to utilize statistical techniques for partitioning the feature space into different tissue classes. This 'feature space classifier' can be either supervised or unsupervised. In this review we will concentrate on the supervised multi-spectral segmentation techniques, reflecting our own research interest. Unsupervised techniques such as those based on fuzzy logic and fuzzy connectivity[21] will not be discussed here. The supervised methods require the operator to generate 'training sets' of data. The training set is generated by sampling 30 to 40 points of each tissue on the images by an expert. These points are plotted in the feature space and a feature space classifier is invoked which partitions the feature space, based on the training set[33,34]. The feature space classifier can be either parametric (maximum likelihood method or MLM) or nonparametric (k-nearest neighbours or KNN and Parzen window)[35]. The MLM method assumes a particular distribution of the features, usually a multi-variate Gaussian. Clarke *et al.*[36] have recently compared the parametric and nonparametric techniques and found the KNN technique to be optimum both in terms of accuracy and stability. Parzen technique falls in the same category as the KNN technique and is more appropriate for lower dimensional feature space. Parzen technique also assures convergence for smaller sample size. In all our studies, we utilize Parzen window technique for tissue classification[35]. Although this is a supervised technique in the sense that the operator input is required for generating the training set, Narayana and Borthakur[37] have demonstrated that by performing intensity normalization on all data sets, it is possible to utilize a single 'master' feature map for segmentation of all the images. The use of a master map, therefore, allows for automatic segmentation of MR images, effectively eliminating the operator bias and dramatically reducing the time requirements for segmentation.

Multi-spectral segmentation techniques most commonly utilize dual echo images (approximately density-weighted and T_2-weighted images) as input images[33,34,38]. Some investigators have also utilized other input images such as T_1-weighted[39] and magnetization transfer contrast (MTC) images[40]. While this strategy provides fairly accurate classification of GM, WM, and CSF, it generates a large number of false positive and false negative lesion classifications, mainly due to limited lesion-to-tissue contrast (LTC). Therefore accurate segmentation of lesions requires considerable manual

intervention which introduces significant operator bias and increases the analysis time. Hence, segmentation techniques based on conventional MR images for lesion quantitation met with limited success.

Affirmative images

The quality of lesion quantitation, irrespective of the segmentation technique used, critically depends on the LTC. Many lesions appear in the peri-ventricular regions and experience considerable partial volume averaging with the CSF, which degrades the LTC. Therefore any sequence which suppresses the CSF without a concomitant lesion suppression should improve the LTC. Indeed it was shown that the LTC can be considerably improved by suppressing the CSF through the use of FLAIR (Fluid Attenuation by Inversion Recovery) technique[41]. MS lesions predominantly occur in the WM. Therefore, the LTC can also be improved if the surrounding white matter is suppressed without greatly affecting the intensity of the lesions. This can be realized to some extent by exploiting the differences in the magnetization transfer ratios (MTR) between WM and the lesions[42,43]. Generally the surrounding WM has a higher MTR than the lesion. Therefore, incorporation of magnetization transfer pulse into the imaging sequence preferentially suppresses the WM signal relative to that of the lesion[44]. It is possible to incorporate MTR and CSF suppression into a single imaging sequence and substantially improve the LTC. Bedell *et al.*[45] have developed an imaging sequence which accomplishes this and christened it AFFIRMATIVE (Attentuation of Fluid by Fast Inversion Recovery with MAgnetization Transfer Imaging with Variable Echoes). The AFFIRMATIVE sequence generates four images per slice. These correspond to early and late echo fast spin echo (FSE) images and early and late echo images which incorporate both MTC and FLAIR (FLAIR/MTC images). As a typical example, the four AFFIRMATIVE images from a section of the brain are shown in Figure 1. From this figure the improved LTC in the late echo FLAIR/MTC (*d*) compared to the FSE images (*a* and *b*) can be easily appreciated. In fact, some of the cortical and subcortical lesions which are hardly visible in the FSE images can be clearly seen in the FLAIR/MTC images. Visualization of cortical and sub-cortical MS lesions may be particularly important since these lesions may play an important role in the functional deficit seen in some of the MS patients.

Image pre-processing

Lesion quantitation requires a series of image processing steps. These include image filtration for improving the signal-to-noise ratio (SNR), correcting for the radio frequency (RF) inhomogeneity, and removal of extra-meningeal tissues (EMT) from the images.

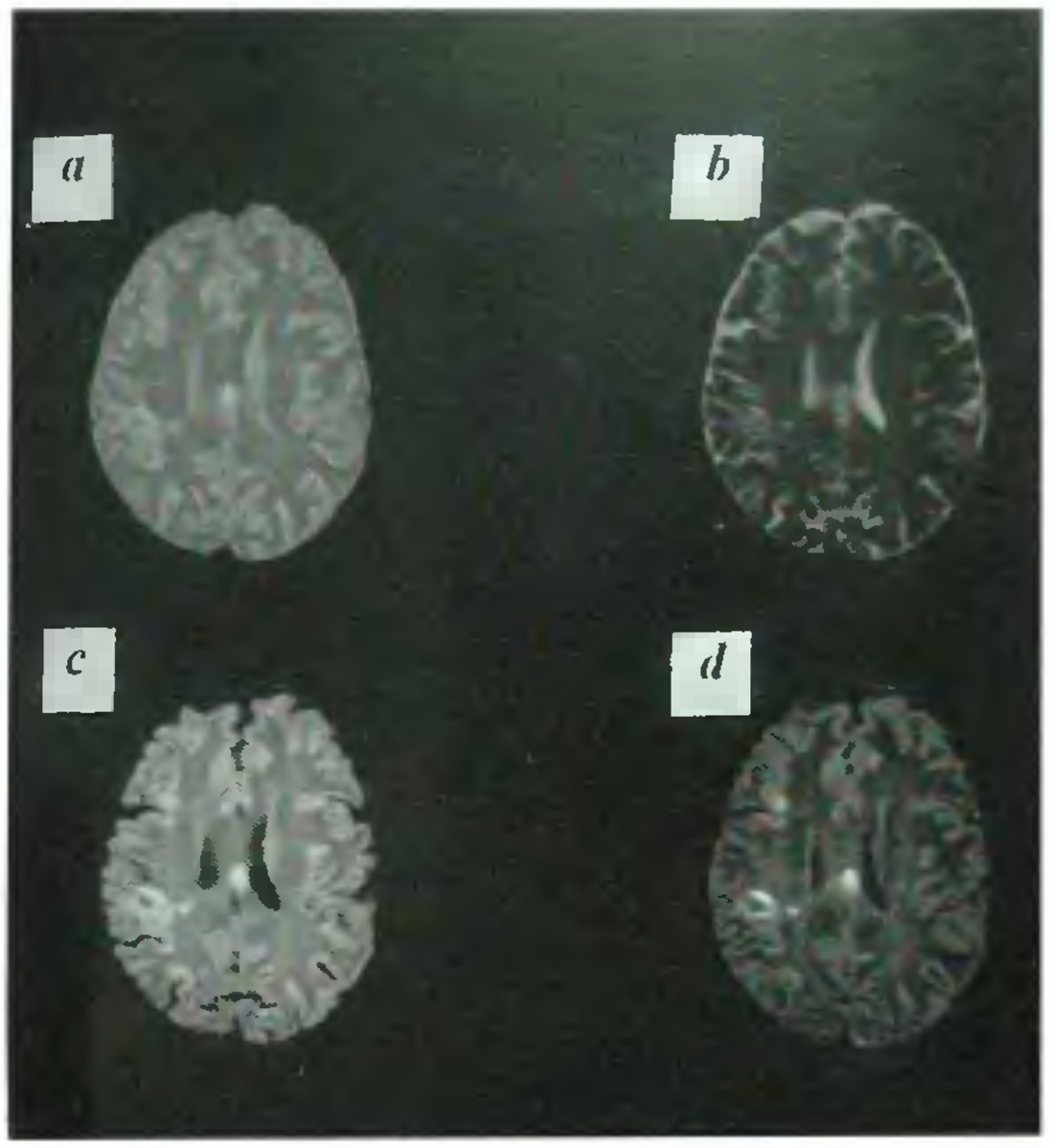

Figure 1 *a–d*. Axial images of a MS brain acquired with the AFFIRMATIVE sequence. ***a***, FSE image with TE = 17 ms; ***b***, FSE image with TE = 102 ms; ***c***, FLAIR/MTC image with TE = 17 ms; and ***d***, FLAIR/MTC image with TE = 102 ms. The other imaging parameters are: TE = 10,000 ms, slice thickness = 3 mm, field-of-view = 240 mm, acquisition matrix of 256 × 128 (image matrix of 256 × 256), number of excitations = 1. The clear visualization of cortical and sub-cortical lesions in the late echo FLAIR/MTC image, ***d***, compared to the FSE images can easily be appreciated. (Reprinted from ref. 45 with permission).

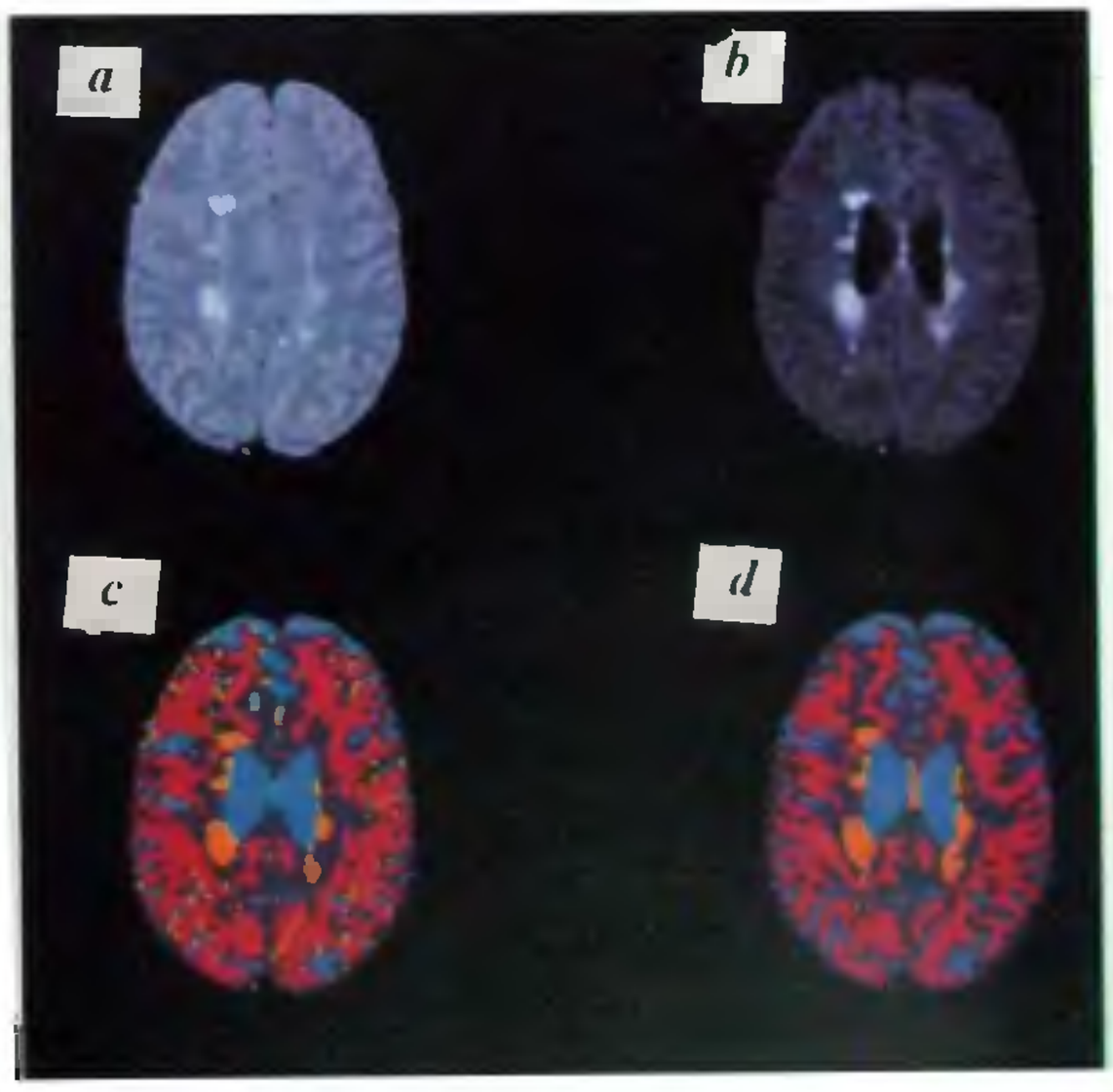

Figure 2 *a–d*. Segmented images based on dual echo FSE, (*c*), and dual echo FLAIR/MTC image, (*d*). WM is represented in pink, GM in grey, CSF in blue, and lesions in yellow. For comparison the early echo FSE, (*a*), and late echo FLAIR/MTC, (*b*), images are also shown. The large number of false positives seen in *b* are mostly eliminated in *c*.

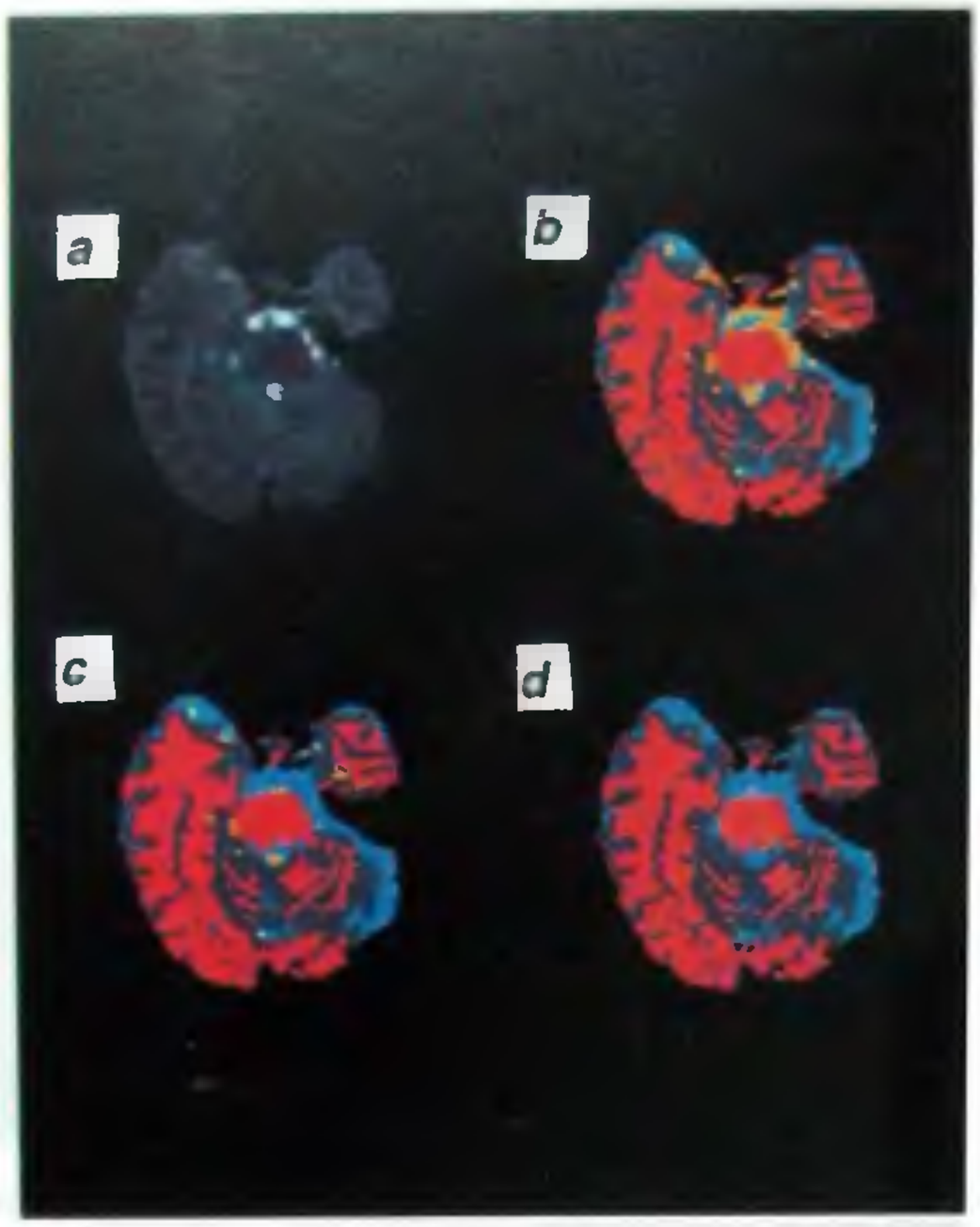

Figure 3 *a–d*. FLAIR/MTC-based segmented images in the posterior fossa region with various corrections. *b*, no correction, *c*, flow-correction; and *d*, flow and ghost correction. For comparison the late echo FLAIR/MTC image is shown in *a*. The elimination of false positives in *d*, can easily be appreciated.

Anisotropic diffusion filter

Poor SNR compromises the quality of segmentation. In a clinical setting it is not practical to perform signal averaging over a long period of time to improve the SNR. Therefore, it is essential to filter the images. However, care has to be exercised in choosing the filter so as not to blur the image and lose information. A number of groups have been using, with considerable success, the anisotropic diffusion filter, originally proposed by Perona and Malik[46]. Studies by Gerig *et al.*[47] and Jackson *et al.*[48] suggest that the application of this filter reduces the low frequency noise without a concomitant blurring of the edges. Application of this filter was found to increase the SNR in the images by a factor of approximately 2.2 (ref. 48). This filter can be set-up so that the parameters characterizing it can be automatically generated from the image[48].

RF inhomogeneity correction

RF inhomogeneity modulates the image intensity that will have a deleterious effect on the segmentation. The importance of RF inhomogeneity in multi-spectral segmentation has been pointed out by a number of investigators[49]. Even though modern RF coils, such as bird cage resonator[50], are designed to produce homogeneous RF field throughout the imaging volume, some RF field inhomogeneity still exists. Studies by Jackson *et al.*[48] suggest that the RF field inhomogeneity, at least in part, is responsible for the observed scan-to-scan and interobserver variation in the segmentation. A number of techniques have been proposed for the RF inhomogeneity correction. Narayana and Borthakur[37] have implemented a relatively simple algorithm, similar to that proposed by Harris *et al.*[51], to correct for the RF inhomogeneity and investigated its effect on the segmentation. This algorithm is based on the fact that the RF inhomogeneity contains only low frequency spatial components that can be filtered out. The smoothed image, following filtration, contains information about the in-plane RF inhomogeneity. However, such a smoothing introduces ringing artifacts around the regions in the image with steep intensity gradients, such as those encountered near the ventricles and the edge of the brain. The first step to circumvent this problem is to identify those pixels which deviate from the mean parenchymal intensity by one standard deviation or more using a histogram analysis. Next, these pixels are replaced by the mean intensity of the brain parenchyma. The resulting images are smoothed with, for example, a 25×25 averaging filter. This smoothed or the blurred image reflects the in-plane RF profile. The anistropically filtered images are divided by this RF profile to obtain the corrected image. All the corrected images are normalized based on the average CSF pixel intensities from a representative data set. Narayana and Borthakur[37] have shown that without the RF correction, the segmentation underestimates the cortical GM and overestimates the WM and that the RF correction reduces both the scan-to-scan and inter-subject variability. A very important consequence of the RF inhomogeneity correction and intensity normalization of the images is that a single feature map can be used for tissue segmentation for all subjects/scans. This procedure, therefore, converts an otherwise semi-automatic technique into an automatic one. Contrary to the conclusions reached by Velthuizen *et al.*[49] that RF correction did not have a significant effect on the segmentation of tumour tissues, we find the RF correction to be very critical for automating the lesion quantitation. As implemented by Narayana and Borthakur[37], the RF correction scheme does not compensate for the RF field variation along the slice selective direction. Correcting for the RF homogeneity in all dimensions requires a complicated algorithm.

Image stripping

In multispectral segmentation, the extra-meningeal tissues (EMT) are a major source of false positives. Therefore removal or stripping of the EMT from the images is

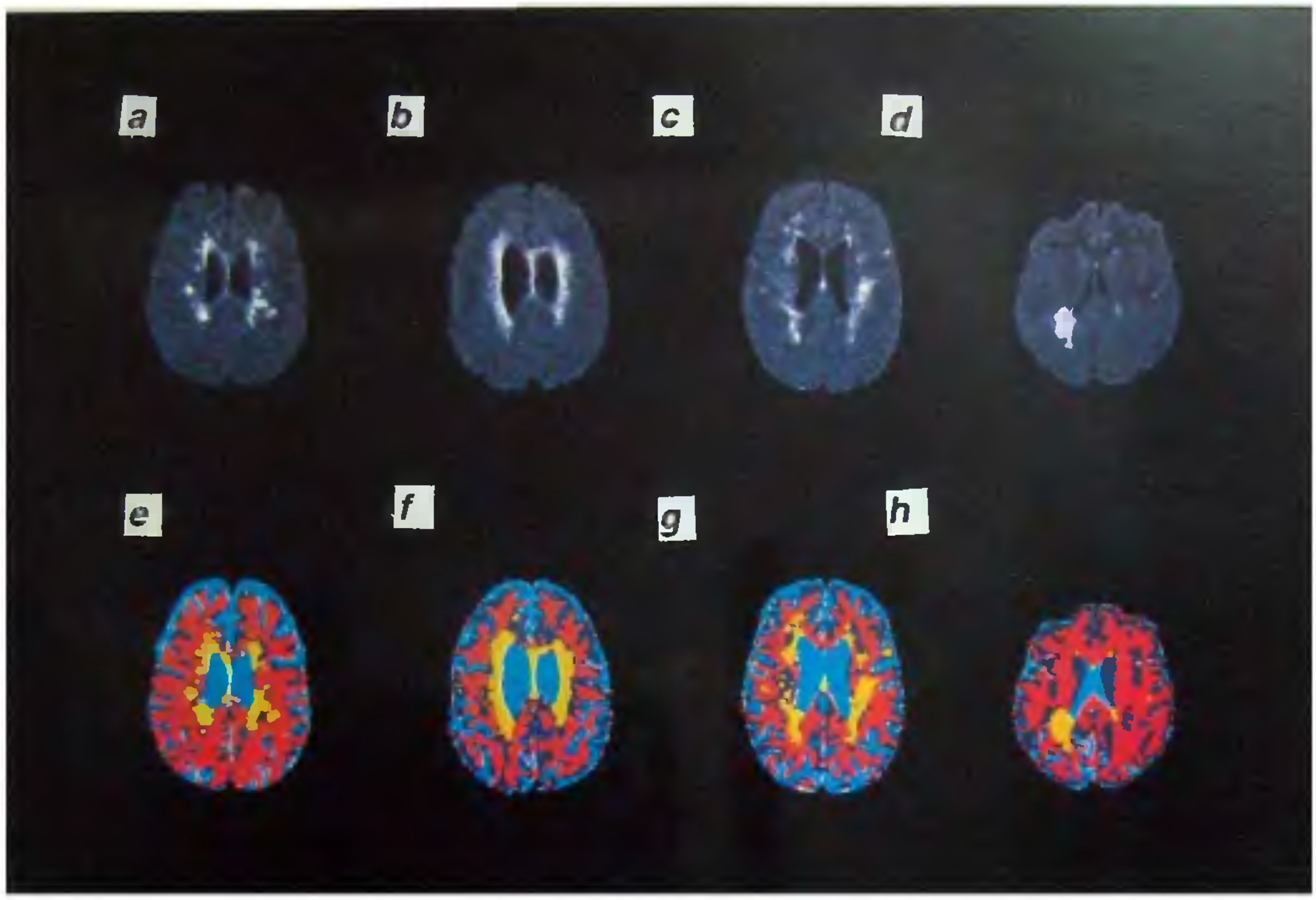

Figure 4. Segmented images from four patients from four different centers (bottom row) automatically generated using a single 'master' feature map. The corresponding late echo FLAIR/MTC images are shown in the top row. The excellent segmentation quality can easily be appreciated in these images.

a crucial operation that needs to be performed prior to segmentation. Automatic removal of the EMT is a non-trivial problem. Traditionally removal of EMT is realized by using a variety of semiautomatic techniques as described by Cline *et al.*[52], Brummer *et al.*[53] and Ardekani *et al.*[54] have recently described automatic techniques for the removal of EMT based on one or two echo images. The relatively poor contrast seen on their images mandated these investigators to incorporate a number of heuristics, which are not always valid, resulting in a significant error in the EMT removal. Recently Bedell and Narayana[55] have implemented an algorithm for automatic removal of EMT based on the multi-spectral segmentation technique using the AFFIRMATIVE images, which exhibit excellent parenchyma-to-EMT contrast, as the input data. Their studies demonstrate that this technique works well even in very difficult regions, namely those near the vertex and optic nerve, and the inferior temporal gyri.

Segmentation

With all the necessary pre-processing steps completed, it is possible to segment AFFIRMATIVE images for determining the lesion load. As indicated earlier, the AFFIRMATIVE sequence generates four images per slice. It is therefore possible to generate a 4D feature map for segmentation. However, segmentation based on a 4D feature space taxes even very powerful computers. Instead, it is more efficient to perform segmentation based on multiple 2D feature maps with various combinations of images. In order to evaluate the improvement in the quality of segmentation by incorporating the FLAIR and MTC, initial segmentation was performed using the early and late echo FSE images. This is quite similar to the dual echo images which formed the basis images in a number of earlier multi-spectral segmentation techniques. Segmentation was also performed using the early and late echo FLAIR/MTC images. The results of the segmentation along with the input images at the level of lateral ventricles are shown in Figure 2. As can easily be appreciated from this figure, the FSE-based segmentation produces a large number of false positive and false negative lesion quantitation. The number of false classifications has dramatically decreased in the FLAIR/MTC-based segmented images.

Flow correction

Segmentation based on FLAIR/MTC images works well for regions superior to the lateral ventricles. But it is far

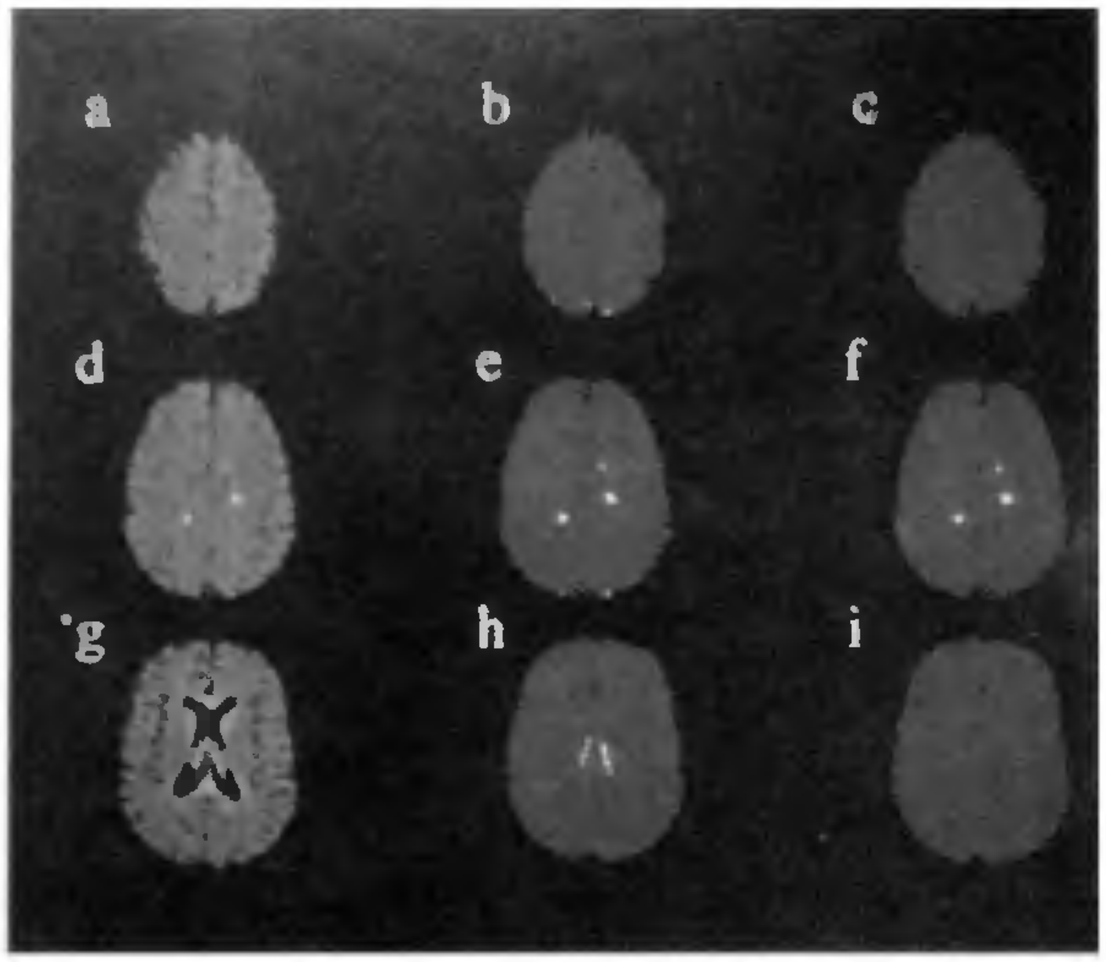

Figure 5. Automatic segmentation of enhancements at different brain locations in a MS patient. The T_1-weighted images acquired with the pulse sequence described in the text are shown in the first column. The imaging parameters are: TE = 25 ms, TR = 800 ms, slice thickness = 3 mm, acquisition matrix of 256 × 128 (image matrix of 256 × 256), FOV = 240 mm, number of excitations = 0.5. The enhancing vasculature was suppressed using marching sat bands and gradient dephasing techniques. Automatic identification without post-processing corrections is shown in the second column. The enhancing choroid plexus can be seen in these images. Segmented images, following the post-processing correction described in ref. 71, are shown in the third column. Note the elimination of non-lesion enhancing structures in these images. (Reprinted from ref. 71 with permission).

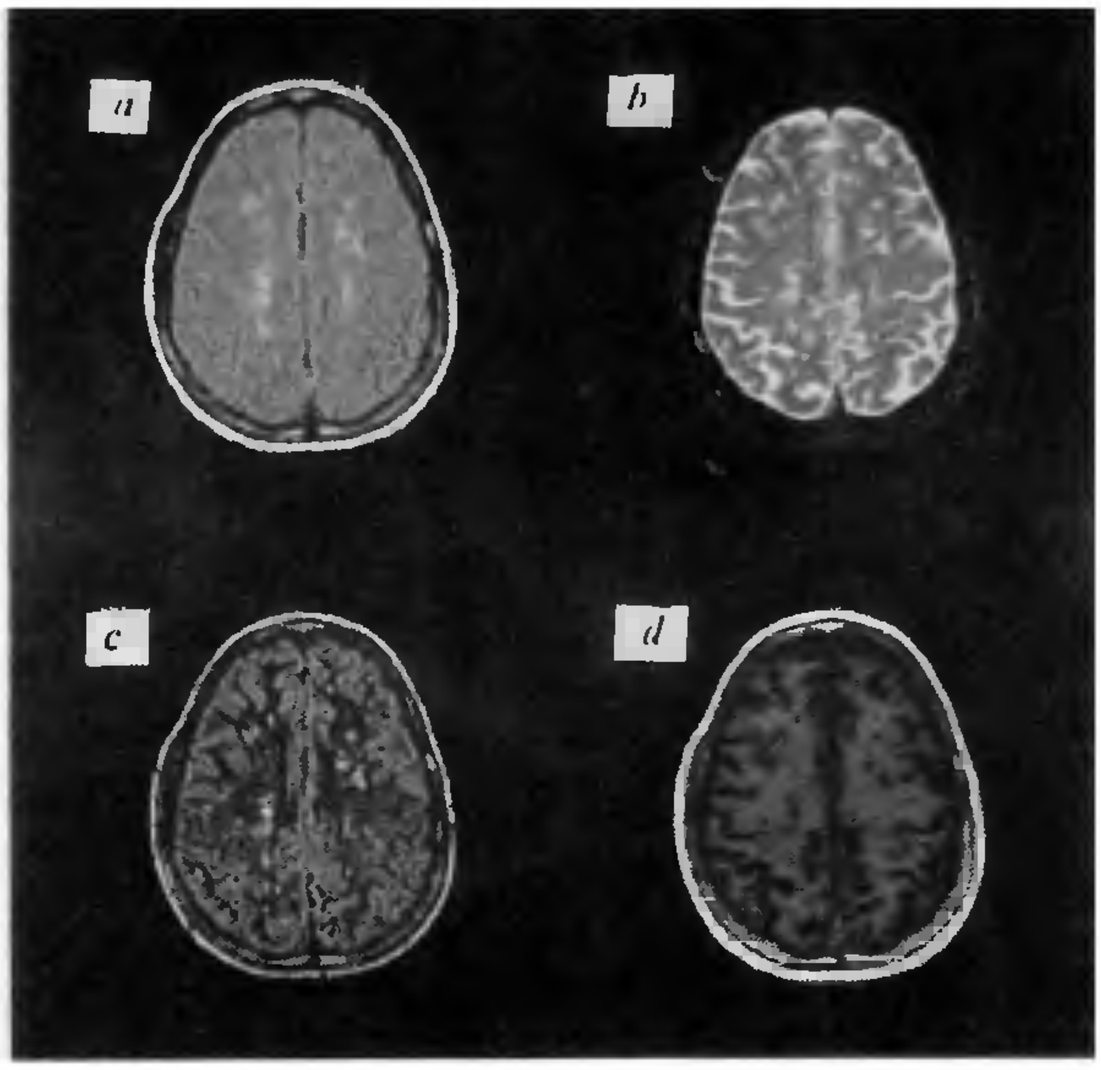

Figure 6 *a–d*. Quadruple contract images from a MS brain. The images correspond to *a*, short echo FSE; *b*, long echo FSE; *c*, WM/CSF suppressed, and *d*, GM/CSF suppressed. The imaging parameters are: TE = 10 ms, TR = 10,000 ms, echo train length = 12, slice thickness = 3 mm, acquisition matrix of 128 × 256 (image matrix of 256 × 256), FOV = 240 mm, number of excitations = 1.

from satisfactory in the slices inferior to the lateral ventricles. A careful inspection of the segmentation results indicates the prevalence of false positives in the regions with substantial vascular and CSF flow such as insula, posterior fossa, and cerebellum. As demonstrated by Bedell *et al.*[45], it is possible to automatically identify and eliminate these regions using the MR flow images. In particular, it is possible to identify both vascular flow (coherent flow) and CSF flow (incoherent flow) on 3D phase contrast images. Incorporation of the flow information into the segmentation process considerably reduces the number of false positives even in the difficult regions such as posterior fossa, as shown in Figure 3.

Even after the incorporation of flow information into segmentation, the segmented images still show a few false positives arising from flow ghosts which mimic lesions. As Bedell *et al.*[45] have demonstrated, it is possible to automatically identify and eliminate these ghost-induced artifacts. The improvement in the segmentation following the correction for the flow ghosts is shown in Figure 3 *d*. As can be appreciated, at least visually, the quality of segmentation appears fairly good after correcting for the flow and ghost-induced artifacts.

As indicated earlier, with this technique, generation of a single master map is adequate for segmenting all images generated on different patients. This can be seen in Figure 4 which shows the FLAIR/MTC and segmented images from different centers, generated using a single feature map. Finally, Wolinsky *et al.*[56] applied this technique in quantitating lesions in 718 patients from 27 centers, the largest study of its kind, with excellent results.

Evaluation and validation

Quantitative evaluation of any segmentation technique is a non-trivial problem. The quality of segmentation in general is evaluated in terms of stability (i.e. inter- and intra-rater variability) and accuracy. The multi-spectral segmentation based on AFFIRMATIVE images is fully automatic except for the initial generation of the master feature map and, therefore, the inter- and intra-operator variabilities have little meaning. However, evaluation of the accuracy of any lesion quantitation is much more difficult simply because the true lesion volumes are not known. While reasonable estimation of the accuracy of lesion quantitation can be realized using phantoms, such as the one proposed by Jackson *et al.*[38], it hardly mimics the complex neuro-anatomy and physiology. Therefore,

it is not uncommon to evaluate the accuracy of segmentation techniques by comparing the segmentation results with those generated manually by an expert. Wolinsky *et al.*[56] have reported such a validation using images on 185 patients. These authors report a correlation coefficient of 0.98 ($P < 0.01$). To the best of our knowledge, this is the largest study of its kind that has been ever performed for validating any segmentation technique.

Quantitation of enhancing lesions

An important aspect of the pathophysiology of acute MS lesions is the presence of perivenous inflammation and associated disruption of regional blood–brain barrier. This loss of local blood–brain barrier can be visualized as an enhancement on T_1-weighted MRI following the administration of a paramagnetic contrast agent such as gadopentate dimeglumine (Gd). Some of these enhancing lesions are clinically symptomatic and Gd enhancement is used as a surrogate marker for evaluating the therapeutic efficacy[57]. Correlation between active lesions, as determined on histopathology, and contrast enhancement has been demonstrated[58,59]. It is, therefore, important to determine either the volume and/or the number of enhancing lesions. This is generally realized either using manual[57,60–65], or computer assisted[66,67], and more recently using completely automatic techniques[68–70]. Both visual identification and automated volumetric analysis of enhancing lesions are complicated by other enhancing structures, such as cerebral vasculature and regions such as choroid plexus in which the blood–brain barrier is absent. These regions mimic lesion enhancements. In the automatic technique based on fuzzy connectivity, these false lesions are discarded by the operator[69]. Bedell and Narayana[70] have adapted a new strategy which is based on images generated with a new pulse sequence and post-processing technique for automating the detection of lesion enhancements. The pulse sequence is based on a spin echo sequence which incorporates both stationary and marching saturation bands and gradient dephasing for suppressing enhancements within the cerebral vasculature. The post-processing technique automatically identifies other non-lesion enhancing structures such as choroid plexus. Thus only truly enhancing lesions are identified and quantified in the final segmented images. A typical set of images demonstrating the performance of this technique is shown in Figure 5. Based on a limited number of patient studies, this technique appears to perform well. However, these authors pointed out that this automated technique gives rise to a few false positives. The size of these false positive enhancements, however, appears to be smaller than 3 pixels. These false positives contribute relatively little to the estimated total enhancing volume and, therefore, this technique appears to be useful for computing the total enhancing volume.

Quadruple contrast imaging

A common problem with MRI is the partial volume averaging between different tissues. The partial volume averaging results in both false positive and false negative lesion classifications. Partial volume averaging can be reduced by acquiring thinner slices with smaller pixels. This is achieved by prolonging the acquisition time. In any case, the ultimate attainable resolution is limited by the available SNR. Bedell and Narayana[71] recently implemented a new FSE-based pulse sequence, called quadruple contrast sequence, which reduces the partial volume averaging by simultaneously suppressing CSF and either GM or WM in the image. This pulse sequence is based on the double inversion recovery concept, originally proposed by Redpath *et al.*[72] for a conventional spin echo sequence. The quadruple contrast sequence, as implemented by Bedell and Narayana[71], produces four images for each slice. These are: (1) fast spin echo image (either short or long echo), (2) fast FLAIR image, (3) WM and CSF suppressed image, and (4) GM and CSF suppressed images. A typical example of quadruple contrast images is shown in Figure 6. It is interesting to note that lesions appear hyperintense and more conspicuous in the CSF/WM suppressed images compared to FLAIR/MTC images. The same lesions, however, appear hypointense on the CSF/GM suppressed images. This dramatically different appearance of lesions on different images is expected to generate tight clusters in the feature space and lead to an accurate segmentation. Images generated with this sequence have been so far used only for quantitating GM, WM, and CSF in normal cases.

A very interesting feature of quadruple contrast images is that lesions appear different in different images, perhaps reflecting their pathologic heterogeneity. Thus, this sequence appears to have the potential for not only providing information about the lesion volumes but also about their heterogenous pathology.

Conclusions

In this brief review, we presented techniques that are developed and implemented in our laboratory for quantitating MS lesions. Our research is driven by the need to automate lesion quantitation techniques for use in clinical trials involving the analysis of hundreds of thousands of MR images. This requires the development of novel pulse sequences for improving the LTC and newer analysis techniques for automating the lesion quantitation. In future, it may be possible to noninvasively characterize their pathology based on newer imaging sequences. The clinical implications of such an ability are obvious. While our main interest is in MS, the techniques described above can be easily applied to other focal pathologies.

1. Caviness, V. J., Kennedy, D. N., Makris, N. and Bates, J., *Brain Dev.*, 1995, **17**, 399–408.
2. Caviness, V. J., Kennedy, D. N., Richelme, C., Rademacher, J. and Filipek, P. A., *Cereb. Cortex*, 1996, **6**, 726–736.
3. Watson, C., Jack, C. J. and Cendes, F., *Arch. Neurol.*, 1997, **54**, 1521–1531.
4. Jack, C. J., Petersen, R. C., Xu, J. C., O'Brien, P. C., Waring, S. C., Tangalos, E. G., Smith, G. E., Ivnik, R. J., Thibodeau, S. N. and Kokmen, E., *Ann. Neurol.*, 1998, **43**, 303–310.
5. Paty, D. W., Li, D. K., Oger, J. J., Kastrukoff, L., Koopmans, R., Tanton, E. and Zhao, G. J., *Ann. Neurol.*, 1994, **36**, Suppl. S95–S96.
6. Riahi, F., Zijdenbos, A., Narayanan, S., Arnold, D., Francis, G., Antel, J. and Evans, A. C., *Brain*, 1998, **121**, 1305–1312.
7. Khoo, V. S., Dearnaley, D. P., Finningan, D. J., Padhani, A., Tanner, S. F. and Leach, M. O., *Radiother. Oncol.*, 1997, **42**, 1–15.
8. Tronnier, V. M., Wirtz, C. R., Kanuth, M., Lenz, G., Pastyr, O., Bonsanto, M. M., Albert, F. K., Kuth, R., Staubert, A., Schlegel, W., Sartor, K. and Kunze, S., *Neurosurgery*, 1997, **40**, 891–900.
9. Black, P. M., Moriarty, T., Alexander, E., Stieg, P., Woodward, E. J., Gleason, P. L., Martin, C. H., Kikinins, R., Schwartz, R. B. and Jolez, F. A., *Neurosurgery*, 1997, **41**, 831–842.
10. Anderson, D. W., Ellenberg, J. H., Leventhal, C. M., Reingold, S. C., Rodriguez, M. and Silberberg, D. H., *Ann. Neurol.*, 1992, **31**, 333–336.
11. Paty, D. W., *Can. J. Neurol. Sci.*, 1988, **15**, 266–272.
12. Filippi, M., Horsfield, M. A., Morrisey, S. P., MacManus, D. G., Rudge, P., McDonald, W. I. and Miller, D. H., *Neurology*, 1994, **44**, 635–641.
13. Kappos, L., Stadt, D., Ratzka, M., Keil, W., Schneiderbanger-Grygier, S., Heitzer, T., Poser, S. and Nadjmi, M., *Neuroradiology*, 1988, **30**, 299–302.
14. Kastrukoff, L. F., Oger, J. J., Hashimoto, S. A., Sacks, S. L., Li, D. K., Palmer, M. R., Koopmans, R. A., Petkau, A. J., Berkowitz, J. and Paty, D. W., *Neurology*, 1990, **40**, 479–486.
15. Paty, D. W., Li, D. K. B., Group, U. M. M. S. and Group, I. M. S. S., *Neurology*, 1993, **43**, 662–667.
16. Sipe, J. C., Romine, J. S., Koziol, J. A., McMillan, R., Zyroff, J. and Beutler, E., *Lancet*, 1994, **344**, 9–13.
17. Fillipi, M., Hortsfieldz, M. A., Barkhof, F., Thompson, A. J. and Miller, D. H., *Brain*, 1995, **118**, 1601–1612.
18. Bezdek, J. C., Hall, L. O. and Clarke, L. P., *Med. Phys.*, 1993, **20**, 1033–1044.
19. Clarke, L. P., Velthuizen, R. P., Camacho, M. A., Heine, J. J., Vaidyanathan, M., Hall, L. O., Thatcher, R. W. and Silgiber, M. L., *Magn. Reson. Imaging*, 1995, **13**, 343–368.
20. Bezdek, J. C., Hall, L. O., Clark, M. C., Goldgof, D. B. and Clarke, L. P., *Stat. Methods Med. Res.*, 1997, **6**, 191–214.
21. Udupa, J. K., Wei, K., Samarasekera, S., Miki, Y., van Buchem, M. A. and Grossman, R. I., *IEEE Trans. Med. Imaging*, 1997, **16**, 598–609.
22. Gonzalez, C. F., Swirsky-Sachetti, T., Mitchell, D., Lublin, F. D., Knobler, R. L. and Ehrlich, S. M., *J. Neuroimaging*, 1994, **4**, 188–195.
23. Wicks, D., Tofts, P., Miller, D., du Boulay, C., Feinstein, A. and Sacares, R., *Neuroradiology*, 1992, **34**, 475–479.
24. Kapouleas, I., *Comput. Programs Methods Biomed.*, 1990, **1**, 17–35.
25. Pannizzo, F., Stallmeyer, M., Friedman, J., Jennis, R., Zabriskie, J. and Plank, C., *Magn. Reson. Med.*, 1992, **24**, 90–92.
26. Kapouleas, I., Grossman, R., Kessler, D., Borstein, J., Cohen, J. and Ramer, K., *Neurology*, 1993, **43**, A246.
27. van Walderveen, M., Barkhof, F., Hommes, O., Polman, C., Tobi, H. and Frequin, S., *Neurology*, 1995, **45**, 1684–1690.
28. Vannier, M. W., Butterfield, R. L., Rickman, D. L., Jordan, D. M., Murphy, W. A. and Biondetti, P. R., *Crit. Rev. Biomed. Sci.*, 1987, **15**, 117–144.
29. Vannier, M. W., Butterfield, R. L., Jordan, D., Murphy, W., Levitt, R. and Gado, M., *Radiology*, 1985, **154**, 221–224.
30. Gonzalez, R. C. and Woods, R. E., in *Digital Image Processing*, Addison-Wesley Publishing Company, Inc, Reading, MA, 1992.
31. Wells III, W. M., Grimson, W. E. L., Member, I., Kikinis, R. and Jolesz, F. A., *IEEE Trans. Med. Imaging*, 1996, 4.
32. Kamber, M. and Shinghal, R., *IEEE Trans. Med. Imaging*, 1995, 14.
33. Cline, H. E., Lorensen, W. E., Kikinis, R. and Jolesz, F., *J. Comput. Assist. Tomogr.*, 1990, **14**, 1037–1045.
34. Kohn, M. I., Tanna, N. K. and German, G. T., *Radiology*, 1991, **178**, 115–122.
35. Duda, R. O. and Hart, P. E., in *Pattern Classification and Scene Analysis*, John Wiley and Sons, Menlo Park, CA, 1973.
36. Clarke, L. P., Velthuizen, R. P., Phuphanich, S., Schellenberg, J. D., Arrington, J. A. and Silbiger, M., *Magn. Reson. Imaging*, 1993, **11**, 95–106.
37. Narayana, P. A. and Borthakur, A., *Magn. Reson. Med.*, 1995, **33**, 396–400.
38. Jackson, E. F., Narayana, P. A., Wolinsky, J. S. and Doyle, T. J., *J. Comput. Assist. Tomogr.*, 1993, **17**, 200–205.
39. Vinitski, S., Gonzalez, C., Moamed, F., Iwanaga, T., Knobler, R., Khalili, K. and Mack, J., *Magn. Reson. Med.*, 1997, **37**, 457–469.
40. van Buchen, M. A., Udupa, J. K., McGowan, J. C., Miki, Y., Heyning, F. H., Boncoeur-Martel, M. P., Kolson, D. L., Polansky, M. and Grossman, R. I., *Am. J. Neuroradiol.*, 1997, **18**, 1287–1290.
41. Hajnal, J. V., Bryant, D. J., Kasuboski, L., Pattany, P. M., De Coene, B., Lewis, P. D., Pennock, J. M., Oatridge, A., Young, I. R. and Bydder, G., *J. Comput. Assist. Tomogr.*, 1992, **16**, 841–844.
42. Grossman, R. I., Gomori, J. M., Ramer, K. N., Lexa, F. J. and Schnall, M. D., *Radiographics*, 1994, **14**, 279–290.
43. Grossman, R. I., *Ann. Neurol.*, 1994, **36**, Suppl., S97–S99.
44. Dousset, V., Grossman, R. I., Ramer, K. N., Schnall, M. D., Young, L. H., Gonzalez-Scarano, F., Lavi, E. and Cohen, J., *Radiology*, 1992, **182**, 483–491.
45. Bedell, B. J., Narayana, P. and Wolinsky, J. S., *Magn. Reson. Med.*, 1997, **37**, 94–102.
46. Perona, P. and Malik, J., *IEEE Trans. Pattern Anal. Machine Intelligence*, 1990, **12**, 629–639.
47. Gerig, G., Kubler, O., Kikinis, R. and Jolesz, F. A., *IEEE Trans. Med. Imaging*, 1992, **11**, 221–232.
48. Jackson, E. F., Narayana, P. A. and Falconer, J. C., *J. Magn. Reson. Imaging*, 1994, **4**, 692–700.
49. Velthuizen, R. P., Cantor, A. B., Lin, H., Fletcher, L. M. and Clarke, L., *Med. Phys.*, 1998, **25**, 1655–1666.
50. Hayes, C. E., Edelstein, W. A., Schenck, J. F., Mueller, O. M. and Eash, M., *J. Magn. Reson. Imaging*, 1985, **63**, 622–628.
51. Harris, G., Barta, P., Peng, L., Lee, S., Brettschneider, P., Shah, A., Henderer, J., Schlaepfer, T. and Pearlson, G., *Am. J. Neuroradiol.*, 1994, **15**, 225–230.
52. Cline, H., Dumoulin, C., Hart, J. and Lorensen, W., *Magn. Reson. Imaging*, 1987, **5**, 345–352.
53. Brummer, M. E., Mersereau, R. M., Eisner, R. L. and Lewine, R., *IEEE Trans. Med. Imaging*, 1993, **12**, 153–166.
54. Ardekani, B. A., Braun, M., Hutton, B. F. and Kanno, I., in *Visualization in Biomedical Computing* (ed. Robb, R. A.), SPIE, Buillinghan, WA, 1994, pp. 402–410.
55. Bedell, B. J. and Narayana, P. A., *JMRI*, 1996, **6**, 939–943.
56. Wolinsky, J. S. and Narayana, P. A., *Neurology*, 1998, **50**, S04.004.

57. McFarland, H. F., Frank, J. A., Albert, P. S., Smith, M. E., Martin, R., Harris, J. O., Patronas, N., Maloni, H. and McFarlin, D. E., *Ann. Neurol.*, 1992, **32**, 758–766.
58. Nesbit, G. M., Forbes, G. S., Scheithauer, B. W., Okazaki, H. and Rodriguez, M., *Radiology*, 1991, **180**, 567–574.
59. Katz, D., Taubenberger, J., Cannella, B., McFarlin, D., Raine, C. and McFarland, H., *Ann. Neurol.*, 1993, **34**, 661–669.
60. Harris, J. O., Frank, J. A., Patronas, N., McFarlin, D. E. and McFarland, H. F., *Ann. Neurol.*, 1991, **41**, 548–555.
61. Barhof, F., Hommes, O. R., Scheltens, P. and Valk, J., *Neurology*, 1991, **41**, 1219–1222.
62. Capra, R., Marciano, N., Vignolo, L. A., Chiesa, A. and Gasparotti, R., *Arch. Neurol.*, 1992, **49**, 687–689.
63. Wiebe, S., Lee, D. H. and Karlik, S. *et al.*, *Ann. Neurol.*, 1992, **32**, 643–650.
64. Thompson, A. J., Miller, D., Youl, B., MacManus, D., Moore, S., Kingsley, D., Kendall, B., Feinstein, A. and McDonald, W. J., *Neurology*, 1992, **42**, 60–63.
65. Barkhof, F., Scheltens, P., Frequin, S. T., Nanta, J. J., Tas, M. W. and Volk, J., *Am. J. Roentgenol.*, 1992, **159**, 1041–1047.
66. Smith, M. E., Stone, L. A., Albert, P. S., Frank, J. A., Marlin, R., Armstrong, M., Maloni, H., McFarlin, D. E. and McFarland, H. F., *Ann. Neurol.*, 1993, **33**, 480–489.
67. Frank, J. A., Stone, L. A., Smith, M. E., Albert, P. S., Maloni, H. and McFarland, H. F., *Ann. Neurol.*, 1994, **36**, S86–90.
68. Samarasekera, S., Udupa, K., Miki, Y., Wei, Y. and Grossman, R. I., *J. Comput. Assist. Tomogr.*, 1997, **21**, 145–151.
69. Miki, Y., Grossman, R. I., Udupa, J., Samarasekera, S., van Buchen, M. A., Cooney, B. S., Pollack, S. N., Kolson, D. L., Costantinescu, C., Polansky, M. and Mannon, L. J., *Am. J. Neuroradiol.*, 1997, **18**, 705–710.
70. Bedell, B. J. and Narayana, P. A., *Magn. Reson. Med.*, 1998, **39**, 935–940.
71. Bedell, B. J. and Narayana, P. A., *Magn. Reson. Med.*, 1998, **39**, 961–969.
72. Redpath, T. W. and Smith, F. W., *Br. J. Radiol.*, 1994, **67**, 1258–1263.

ACKNOWLEDGEMENTS. This work was supported in part by the National Institutes of Health Grant #NS31499.